A null mutation of the neuronal sodium channel $Na_V1.6$ disrupts action potential propagation and excitation-contraction coupling in the mouse heart

Sami F. Noujaim,*[,1] Kuljeet Kaur,*[,1] Michelle Milstein,*[,1] Julie M. Jones,[†] Philip Furspan,* Daniel Jiang,* David S. Auerbach,* Todd Herron,* Miriam H. Meisler,[†,2] and José Jalife*[,2,3]

*Center for Arrhythmia Research and [†]Department of Human Genetics, University of Michigan, Ann Arbor, Michigan, USA

ABSTRACT **Evidence supports the expression of brain-type sodium channels in the heart. Their functional role, however, remains controversial. We used global $Na_V1.6$-null mice to test the hypothesis that $Na_V1.6$ contributes to the maintenance of propagation in the myocardium and to excitation-contraction (EC) coupling. We demonstrated expression of transcripts encoding full-length $Na_V1.6$ in isolated ventricular myocytes and confirmed the striated pattern of $Na_V1.6$ fluorescence in myocytes. On the ECG, the PR and QRS intervals were prolonged in the null mice, and the Ca^{2+} transients were longer in the null cells. Under patch clamping, at holding potential (HP) = −120 mV, the peak I_{Na} was similar in both phenotypes. However, at HP = −70 mV, the peak I_{Na} was smaller in the nulls. In optical mapping, at 4 mM $[K^+]_o$, 17 null hearts showed slight (7%) reduction of ventricular conduction velocity (CV) compared to 16 wild-type hearts. At 12 mM $[K^+]_o$, CV was 25% slower in a subset of 9 null *vs.* 9 wild-type hearts. These results highlight the importance of neuronal sodium channels in the heart, whereby $Na_V1.6$ participates in EC coupling, and represents an intrinsic depolarizing reserve that contributes to excitation.—Noujaim, S. F., Kaur, K., Milstein, M., Jones, J. M., Furspan, P., Jiang, D., Auerbach, D. S., Herron, T., Meisler, M. H., Jalife, J. A null mutation of the neuronal sodium channel $Na_V1.6$ disrupts action potential propagation and excitation-contraction coupling in the mouse heart. *FASEB J.* 26, 63–72 (2012). www.fasebj.org**

Key Words: ataxia3 · brain-type sodium channels · hyperkalemia · optical mapping

Channelopathies are an increasingly recognized category of inherited human diseases (1, 2). Missense mutations of Na^+-channel genes have been linked not only to cardiac ion-channel diseases (1, 2) but also to epilepsy, chronic pain, and motor disorders (3, 4). A rare heterozygous null mutation of human *SCN8A*, which encodes the sodium channel $Na_V1.6$, was identified in a 9-yr-old boy with mental retardation, pancerebellar atrophy, and ataxia; 3 additional heterozygotes in the same family exhibited milder cognitive and behavioral defects, including attention deficit hyperactivity disorder (5). However, no studies have been reported to assess the possibility that mutation of $Na_V1.6$ produces adverse consequences in cardiac electrical function.

There are 9 genes for functional voltage-gated sodium-channel α subunits in the human genome (6). Several of these genes, including brain-type genes, are expressed in the heart, and the Na^+-channel subtypes are differentially localized and appear to have differences in functional properties (6, 7). Structurally, Na^+ channels are complexes of a ~260-kDa α subunit in association with smaller β subunits of 33–36 kDa (8). The $Na_V1.5$ sodium-channel gene is strongly expressed in the heart, and for many years it was thought to be exclusively responsible for generating the upstroke of the normal cardiac action potential. However, it has recently become evident that neuronal and skeletal muscle Na^+-channel isoforms are also expressed at low levels in the heart and may contribute to cardiac function (3). Immunolocalization studies have revealed distinct subcellular localization of the various α and β subunits, and it has been proposed that the primary Na^+ channels in ventricular myocytes are composed of $Na_V1.5$ plus β2 and/or β4 subunits in intercalated disks, in addition to $Na_V1.1$, $Na_V1.3$, and $Na_V1.6$ plus β1 and/or β3 subunits in the transverse tubules (9, 10). Functionally, brain-type Na^+ channels are thought to be involved in excitation-contraction (EC) coupling by synchronizing the action potential in the sarcolemmal of the t tubules (11). Such a role, however, remains controversial (12). On the other hand, it has been suggested that tetrodotoxin (TTX)-sensitive brain-type Na^+ channels contribute to automaticity of sinoatrial

[1] These authors contributed equally to this work.
[2] These authors contributed equally to this work.
[3] Correspondence: Center for Arrhythmia Research, University of Michigan, 5025 Venture Dr., Ann Arbor, MI 48108, USA. E-mail: jjalife@umich.edu

doi: 10.1096/fj.10-179770

nodal cells of the mouse heart and may have a role in sinoatrial dysfunction (13). Recently it was shown that $Na_V1.1$ and $Na_V1.6$ are the primary Na^+-channel subunits in the rat sinus node and that heart failure results in their down-regulation (14).

The individual cardiac contributions of $Na_V1.1$, $Na_V1.3$, and $Na_V1.6$ were not distinguished in previous studies, which were carried out in wild-type animals expressing all 3 neuronal channels.

Several global-null mutants of *Scn8a* lacking the $Na_V1.6$ channel in all tissues have been described (15). $Na_V1.6$-null mice exhibit neurological deficits, including tremor, ataxia, and hindlimb paralysis, and do not survive beyond 3 wk of age. Impaired repetitive firing has been shown in cerebellar Purkinje cells and other types of neurons. Reduced size of the heart was described in the null mutant *Scn8a*^{dmu}, but electrophysiological studies of cardiac function were not carried out (16, 17). We have used the ENU-induced null mutant *Scn8a*^{S21P} (18) to determine the consequences of $Na_V1.6$ reduction on cardiac electrical function and EC coupling. In the ataxia 3 mutant mice, chromosomal mapping of the mutant phenotype and allelism testing demonstrated that the mutation is an allele of *Scn8a* (18). Sequencing of the *Scn8a* brain transcript identified the nucleotide change that resulted in the amino acid substitution S21P (18). The effect of this mutation is to trap the Nav1.6 protein in the Golgi, resulting in the absence of channel activity (18). Our approach utilized biochemistry, calcium imaging, patch clamping, and optical mapping to test the hypothesis that $Na_V1.6$ participates in EC coupling and represents an intrinsic depolarizing reserve that contributes to the maintenance of cardiac excitation.

MATERIALS AND METHODS

Animals

Experiments were carried out with the approval of the Unit of Laboratory Animal Resources at the University of Michigan. Wild-type (WT) littermate and null mice between 19 and 21 d of age were used in this study. Before removal of the heart *via* thoracotomy, the mice were heparinized (5 U/g, i.p.) and then deeply anesthetized with Avertin (0.05 ml/g, i.p.).

$Na_V1.6$ mRNA analysis by RT-PCR and sequencing

Hearts were removed and washed in RNase/DNase free ice-cold PBS. Isolated hearts were saved in RNA stabilizing agent (Ambion, Austin, TX, USA) until further use. For isolated cells, the myocytes were allowed to attach on laminin-coated dishes for 2 h to remove nonmyocytes. After 2 h, cardiac myocytes were washed with PBS and lysed with lysis buffer to isolate RNA and analyze the expression of $Na_V1.6$ transcript. Isolated RNA was treated with DNase. cDNA was synthesized from 2 μg of total RNA with Oligo dT primers using the SuperScript III First-Strand Synthesis System from Invitrogen (Carlsbad, CA, USA) and then subjected to PCR using Clontech titanium taq PCR Kit (Clontech, Mountain View, CA, USA). Sense (5′-AAGTGGACAGCCTATGGCTTCGTC-3′) and antisense (5′-AGCCAGAAGATGAGACACACCAGC-3′) primers (5 pmol) for $Na_V1.6$ were used in PCR. These primers terminate on nucleotides that are specific for this member of the sodium-channel family and amplify a cDNA fragment containing exons 17–19. No-template controls and no-RT controls were run during each experiment to detect any RNA and/or DNA contamination. Samples were denatured at 94°C for 1 min, followed by 35 cycles of denaturation at 94°C for 30 s, annealing at 60°C for 30 s, and extension at 68°C for 1 min, then a final extension at 68°C for 3 min. The PCR product (5 μl) was analyzed on a 2% agarose gel by electrophoresis. The PCR product was cleaned and sequenced using above-mentioned primers for $Na_V1.6$ at the University of Michigan DNA sequencing core.

Mouse ventricular myocyte isolation

On removal of the heart, we proceeded with the enzymatic digestion of the lower 2/3 ventricular region (apex), as described previously (19). Myocytes were resuspended in buffer containing 10% bovine calf serum and $CaCl_2$ (12.5 μM), and $[Ca^{2+}]$ was increased to 1 mM. Cells were used for morphological assessment, immunohistochemistry, electrophysiological recording, and Ca^{2+} imaging within 8 h after isolation.

Cell size measurement

Morphological measurements (length, width) of plated cells were collected using digital photomicroscopy and the imaging program AxioVision (Zeiss) on a Zeiss inverted microscope with a ×10 or ×20 objective (Carl Zeiss, Oberkochen, Germany). No significant differences were observed in length or width between live and fixed cells for any of the groups; all subsequent measurements were then conducted on fixed cells. Cells were selected for measurement if they showed no obvious sign of damage.

Immunocytochemistry

Isolated cells were plated on laminin-coated glass coverslips, fixed with 4% paraformaldehyde (10 min), permeabilized with 0.1% Triton X-100, and washed with PBS. For sections, hearts were incubated in 30% sucrose solution overnight at 4°C. Endogenous mouse immunoglobulin was blocked using a mouse-on-mouse (anti-mouse Ig) blocking reagent (M.O.M. kit; Vector Laboratories, Burlingame, CA, USA) for 1 h at room temperature. Cells were further blocked for 1 h with 5% normal donkey serum in PBS (containing 0.1% Triton X-100), and subsequently incubated with primary antibodies overnight at 4°C. After washing, donkey secondary antibodies (anti-mouse and anti-rabbit) conjugated to DyLight fluorophores (488, 549; Jackson ImmunoResearch Laboratories, West Grove, PA, USA) were added for 1 h. Nuclei were stained with 100 μM 4′-6-diamidino-2-phenylindole (DAPI) and washed, and coverslips were mounted to microscope slides using ProLong Gold Anti-Fade Mounting Kit (Molecular Probes, Eugene, OR, USA). Immunofluorescence was examined with a Nikon Eclipse Ti inverted confocal microscope with a ×63/1.2-NA oil objective (Nikon Inc., Tokyo, Japan), at ambient temperature. Nonconfocal images were obtained using conventional fluorescence with the Apotome system (Zeiss). The antibodies used were rabbit anti-$Na_V1.6$ (Alomone, Jerusalem, Israel) and monoclonal anti-sarcomeric alpha actinin (Sigma-Aldrich, St Louis, MO, USA). In neurons from *Scn8a*-null mice, the Alomone antibody cross-reacts with the other abundant neuronal sodium channels (18), but in cardiomyoctes, we observed specific staining of $Na_V1.6$ (see below).

Patch-clamp experiments

Whole-cell membrane currents were recorded from ventricular myocytes at room temperature (20–22°C) using the patch

clamp (Axopatch 700B amplifier; Axon Instruments, Foster City, CA, USA); settings and properties have been described elsewhere (20, 21). In one set of experiments, I_{Na} was measured in low $[Na^+]_o$ (5 mM) to reduce I_{Na} and improve voltage control. Low-resistance (1.6±0.1 MΩ) patch pipettes were used. Access resistance was compensated to 1–2 MΩ. Input resistance was 0.4–1 GΩ. Appropriate whole-cell capacitance and series resistance compensation were applied, along with leak subtraction. Brain-type sodium channels have steady-state inactivation and activation curves between 15 and 25 mV more positive than $Na_V1.5$ (22). Thus, brain-type sodium channels have greater availability at depolarized ranges of membrane potential. For *I-V* relationships, cells were held at different holding potentials (HP; −120 and −70 mV) and stepped to a range of potentials (−100 to +30 mV in 5-mV increments for HP=−120 mV, and −60 to +30 mV for HP=−70 mV) for 100 ms each. In a second set of experiments, 100 nM TTX-sensitive sodium currents (brain-type isoforms) were measured at 50 mM $[Na^+]_o$ and at the holding potential of −70 mV, in the presence of 1 mM Cd^{2+} to selectively block $Na_V1.5$ (23). In a subset of these experiments, [TTX] was increased to 1 μM.

ECG recording

Lead II ECG in restrained, conscious animals was recorded and digitized (1.2 kHz) using custom-made software in LabView (National Instruments, Austin, TX, USA) and a Biopac Systems amplifier (DA100C) and digitizer (IPS100C; Biopac Systems, Santa Barbara, CA, USA).

Optical mapping of the whole heart

The heart was rapidly excised through thoracotomy, connected to a Langendorff-perfusion system, and perfused with warm oxygenated Tyrode's solution as described earlier (24–26) and allowed to equilibrate for 10 min. We used Di-4-ANEPPS and a CCD camera (64×64 pixel; spatiotemporal resolution 109 μm, 1 kHz) and mapped the epicardial anterior surfaces of the ventricles. Further details have been presented elsewhere (24–27). Here, 7 μM blebbistatin was used to prevent contraction. Sixteen WT and 17 null hearts were initially perfused with 4 mM $[K^+]_o$ Tyrode's solution. In a subset of 9 hearts in both phenotypes, the $[K^+]_o$ was raised to 8, 10, and 12 mM, for 15 min at each $[K^+]_o$. At the ends of the 15-min periods, pacing was done with a bipolar, silver-tip stimulation electrode placed on the apex (3-ms pulses, ×2 diastolic threshold, cycle lengths of 140 and 80 ms), and movies were recorded. We generated activation and APD maps by calculating, for each pixel, the activation time or the APD at 80% repolarization during pacing at 140 and 80 ms. To compute CV, the magnitude of local conduction vectors was determined on the basis of the activation times of surrounding pixels as described elsewhere (24).

Calcium imaging

Briefly, cell suspensions were incubated with cell-permeant rhod-2AM calcium indicator (10 μM; Molecular Probes) for 10 min at room temperature and then washed to remove excess dye. Fluorescence was expressed as $\Delta F/F_0 = (F - F_0/F_0)$, where F is the fluorescence at any given time and F_0 is the baseline fluorescence value. Nonconfocal calcium was imaged at 200 Hz in individual cells using an inverted Zeiss microscope equipped with temperature control and a Redshirt Imaging camera (Redshirt Imaging, Decatur, GA, USA). The cells were paced at 1 Hz.

Statistics

One-way ANOVA with Bonferroni correction and *t* test were used as appropriate. For the hyperkalemia experiments, we used the Multivariate Mixed procedure in the SAS package (SAS Institute, Cary, NC, USA) in consultation with the University of Michigan Center for Statistical Consultation and Research. We indicate in the text and figure legends the statistical test used and whether data are averages ± SE or SD.

RESULTS

Morphological assessment

Macroscopic examination revealed that $Na_V1.6$-null hearts were small compared with WT littermates at 18 d of age. Previous studies noted that the reduction in heart size is proportional to the overall reduction in body weight (16, 17). Since $Na_V1.6$ is a neuronal sodium channel, we investigated whether the nerve supply to the ventricles was altered in the null hearts compared to WT littermates using acetylcholinesterase precipitation reaction (28). Macroscopically, the epicardial innervation of 4 null hearts did not appear to be altered when compared with 4 WT hearts (data not shown). On the other hand, the ventricular myocytes of the null mouse (**Fig. 1*Ab***) were appreciably smaller than those of WT littermates (Fig. 1*Aa*). Morphometric quantification demonstrated that the ventricular cardiomyocytes of 4 null hearts had significantly reduced length (Fig. 1*Ac*) and width (Fig. 1*Ad*) compared to 3 WT hearts. Figure 1*B* compares representative confocal images of the t-tubule network of littermate WT and null myocytes. The images of these live myocytes were stained with wheat-germ agglutinin (Fig. 1*Ba*, *b*) or the lipophilic dye di-8-ANEPPS (Fig. 1*Bc*, *d*). Figure 1*Be*, *f* shows fluorescence intensity profiles along the longitudinal axis of each cell stained with di-8-ANEPPS. Figure 1*Bg*, *h* shows the respective spectra obtained by fast Fourier transformation of the fluorescence profiles. The t-tubule network is apparent in both WT and null cardiomyocytes, with a regular fluorescence profile (peaks at ~2 μm intervals). This pattern was similar in cells from 3 WT and 3 null hearts and is consistent with other studies in rodents (29). In addition, membrane capacitance was decreased in null (72±2.3 pF) compared to WT (83±5.4 pF; $P < 0.05$; N=4, n=10); the resting membrane potential in WT was −77.25 ± 0.76 (N=3, n=6) and in null −75.13 ± 1.18 (N=3, N=6).

Characterization of *Scn8a* transcripts in the heart

The *Scn8a* gene contains alternative exons 18N and 18A that exhibit tissue-specific splicing (30). Transcripts containing exon 18A encode the full-length channel and in previous studies were shown to be restricted to brain. Because of the in-frame stop codon in exon 18N, transcripts in non-neural cells encode a truncated, 2-domain protein (30). This alternative splicing pattern was thought to restrict active $Na_V1.6$ channels to neu-

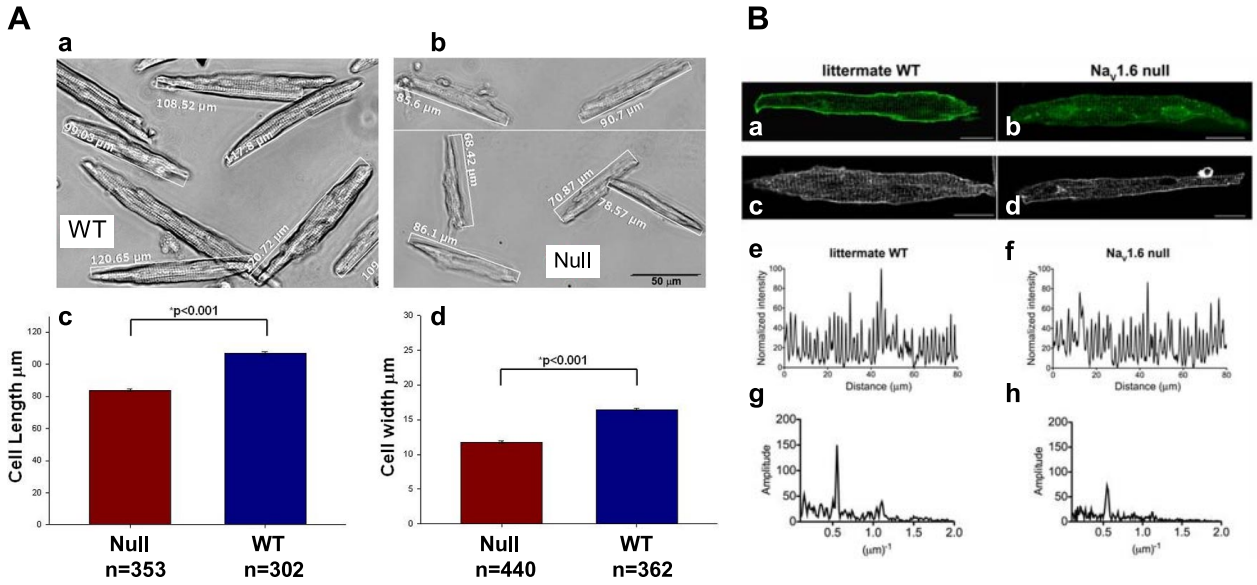

Figure 1. Assessment of cardiomyocyte length and width in $Na_V1.6$ mutant and WT mice and the profile of the t-tubular network. *A*) *a, b*) Cell morphology. *n* = total number of cells from 3 WT (*a*) and 4 null hearts (*b*). *c, d*) Cell length (*c*) and width (*d*); data are averages ± SE, *t* test. *B*) Membrane staining showing t-tubule network in myocytes from WT (*a, c, e, g*) and from $Na_V1.6$-null mice (*b, d, f, h*). *a, b*) Wheat-germ agglutinin. *c, d*) Lipophilic dye di-8-ANEPPS. *e, f*) Fluorescence intensity profiles along the longitudinal axis of each cell stained with di-8-ANEPPS. *g, h*) Fast Fourier transformation of the fluorescence profiles. Scale bars = 50 µm (*A*); 20 µm (*B*).

rons; however, *Scn8a* transcripts in heart have not previously been characterized. To specifically amplify $Na_V1.6$ transcripts in the presence of $Na_V1.5$ and the other brain-type channels, we designed a gene-specific forward primer in exon 17 and reverse primer in exon 19 terminating in nucleotides that differ between $Na_V1.6$ and the other sodium channels. Using these primers, we detected 3 *Scn8a* transcripts in heart containing exon 18A, exon 18N, or skipping both (Δ18; **Fig. 2*A***). The inclusion of exon 18A was confirmed by sequencing the PCR product isolated from the gel. This is the first demonstration that $Na_V1.6$ transcripts encoding full-length protein are expressed in the heart and provides important validation for the detection of $Na_V1.6$ by immunostaining (see below). We also examined $Na_V1.6$ transcripts in isolated adult cardiomyocytes. PCR products from isolated myocytes, whole heart, and brain were amplified from 100 ng of RNA (Fig. 2*B*). These data demonstrate directly that full-length $Na_V1.6$ transcripts are present in the ventricular myocytes.

Immunolocalization of $Na_V1.6$

Previous studies reported that $Na_V1.6$ protein is localized to the t tubules of the mouse cardiac myocyte, but these studies did not include the null control to confirm the specificity of immunostaining (9, 11). After confirming the presence of the full-length coding transcript of *Scn8a* in the heart, we conducted immunolocalization experiments on WT and mutant heart. Immunofluorescence in single cells from WT heart confirmed the localization of $Na_V1.6$ in a t-tubular pattern (**Fig. 3*A***, left panel). $Na_V1.6$ immunofluorescence is shown in red, and α-sarcomeric actinin staining is shown in green. In WT, but not null, myocytes, $Na_V1.6$ exhibits a striated staining pattern that colocalizes with α-actinin (Fig. 3*A*). In *Scn8a*-null myocytes, no specific staining pattern is observed with antibodies for $Na_V1.6$ although actinin staining is normal (Fig. 3*A*, right panel). In addition, the intensity profiles along the indicated arrows (Fig. 3*A*) show that $Na_V1.6$ fluorescence pattern colocalizes with that of actinin in an alternating manner, demonstrating the presence of $Na_V1.6$ in the t tubules of the WT, but not in the null myocyte. The confocal microscope laser settings were identical for all images.

Functional expression of $Na_V1.6$ in the mouse heart

As an initial approximation to estimate the contribution of $Na_V1.6$ to I_{Na} in cardiac ventricular myocytes, we compared the *I-V* relations of WT *vs.* null ventricular myocytes at 5 mM $[Na^+]_o$ and 2 different HPs: −120 mV (**Fig. 4*A***) and −70 mV (Fig. 4*B*). Our rationale for these experiments was based on the fact that the range of inactivation voltages of brain-type Na^+ channels is significantly more positive than $Na_V1.5$ (3, 22); therefore, at −70 mV, the $Na_V1.5$ channels are largely inactivated. In Fig. 4*A*, at HP = −120 mV and 5 mM $[Na^+]_o$, peak inward I_{Na} was similar in the two phenotypes. However, at HP = −70 mV (Fig. 4*B*), the peak inward I_{Na} was smaller in null compared to WT cells (3±0.3 pA/pF, N=2, n=4 *vs.* 5.5±0.28 pA/pF, N=2, n=5, P<0.05, ANOVA). To further distinguish between $Na_V1.5$ and $Na_V1.6$, we used the channel blocker TTX. Brain-type Na^+ channels, including $Na_V1.6$, are sensitive to nanomolar blocking concentrations (100 nM) of

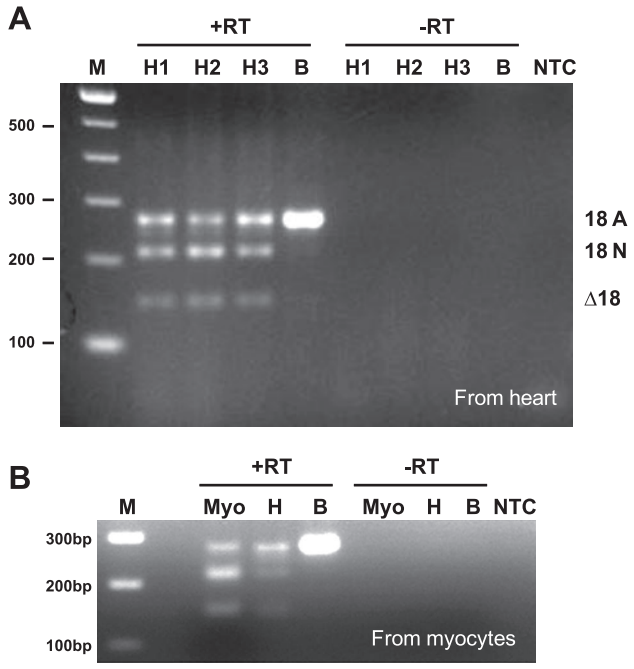

Figure 2. Transcripts of *Scn8a* containing exon 18A and encoding full-length protein in mouse heart and ventricular myocytes. *A*) First-strand cDNA from heart (1 μg) and brain (0.1 μg) was amplified by PCR. PCR products (5 μl) were electrophoresed through 2.5% agarose and visualized by ethidium bromide fluorescence. H1–H3, cDNA from 3 different hearts; NTC, no template control; B, brain as a positive control for the 18A splice form encoding the full-length $Na_V1.6$ protein (35 cycles). *B*) *Scn8a* transcripts in isolated adult cardiac myocytes (Myo) from WT mouse hearts. Positions of the RT-PCR products containing exon 18A, 18N, and skipping exon 18 (Δ18) are shown at right in panel *A*.

TTX, whereas cardiac-type channels require TTX concentrations in the micromolar range to be fully blocked (20, 21). On the other hand, $Na_V1.5$ can be readily blocked by Cd^{2+} at much lower concentrations than brain-type Na^+ channels (23). Therefore, we conducted a second set of experiments to compare the density of the TTX-sensitive I_{Na} in WT *vs.* null myocytes in the continuous presence of 1 mM Cd^{2+}, which enabled us to raise the $[Na^+]_o$ to 50 mM, while still maintaining voltage control. Before TTX, the peak inward I_{Na} was significantly smaller in null cells (Fig. 4*D*) than WT cells (Fig. 4*C*; 3.4±0.6 pA/pF, N=5, n=9 *vs.* 8.9±1 pA/pF, N=4, n=10, P<0.05, ANOVA). After addition of 100 nM TTX, the peak currents decreased to 1.5 ± 0.5 pA/pF in null myocytes (Fig. 4*D*) and 3.4 ± 0.4 pA/pF in WT (P<0.05; Fig. 4*C*). After addition of 1 μM TTX, the current was reduced to 1.5 ± 0.04 pA/pF (N=2, n=4) and 1.2 ± 0.01 pA/pF (N=3, n=5) in WT and null myocytes, respectively. The $V_{1/2}$ of inactivation in WT and null myocytes was −72.2 and −73.1 mV, respectively, and the slope factor was the same in both phenotypes at 9.3 (Fig. 4*E*). For activation, the $V_{1/2}$ and the slope factor in WT and null myocytes were −26.8 mV and 27.9 (Fig. 4*E*). In Fig. 4*F*, the 100 nM TTX-sensitive current obtained from the data in Fig. 4*C*, *D* was significantly smaller in null than WT cells (2.6±0.5 pA/pF *vs.* 5.8±0.7 pA/pF, P<0.05, ANOVA). Altogether, these experiments support the presence of functional $Na_V1.6$ channels in the mouse ventricular myocytes.

Reduced $Na_V1.6$ results in an altered ECG phenotype

We recorded ECGs (lead II) in nonanesthetized, gently restrained conscious WT and null mice. **Figure 5*A*** shows representative recordings of a single sinus beat in a WT mouse (left panel) and in a null mouse (right panel). The PR interval is prolonged and the QRS is wider in the null mouse. Superposition of QRS-T complexes from mice in Fig. 5*B* illustrates the QRS prolongation in the $Na_V1.6$ mutant mouse. The bar graph in Fig. 5*C* quantifies the PR and QRS intervals from 8 WT and 9 null mice. Both intervals were prolonged in the $Na_V1.6$ mutant animals. The PR interval was 30 ± 3.7 ms in null, compared with 42 ± 6.7 ms in WT ($P < 0.05$), and the QRS was 15 ± 3.8 ms

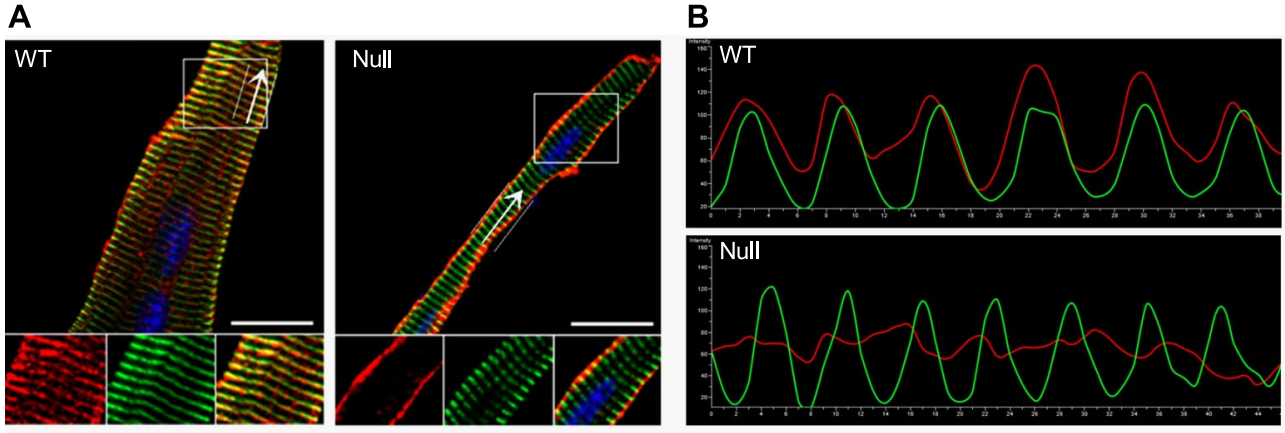

Figure 3. Immunofluorescent patterns of $Na_V1.6$ and actinin. *A*) Immunofluorescent pattern of $Na_V1.6$ (red) and actinin (green) in isolated cardiac myocytes from WT and $Na_V1.6$-null mice. Boxed areas are magnified in bottom panels. *B*) Fluorescence intensity profiles along arrows in panel *A*. Scale bars = 20 μm.

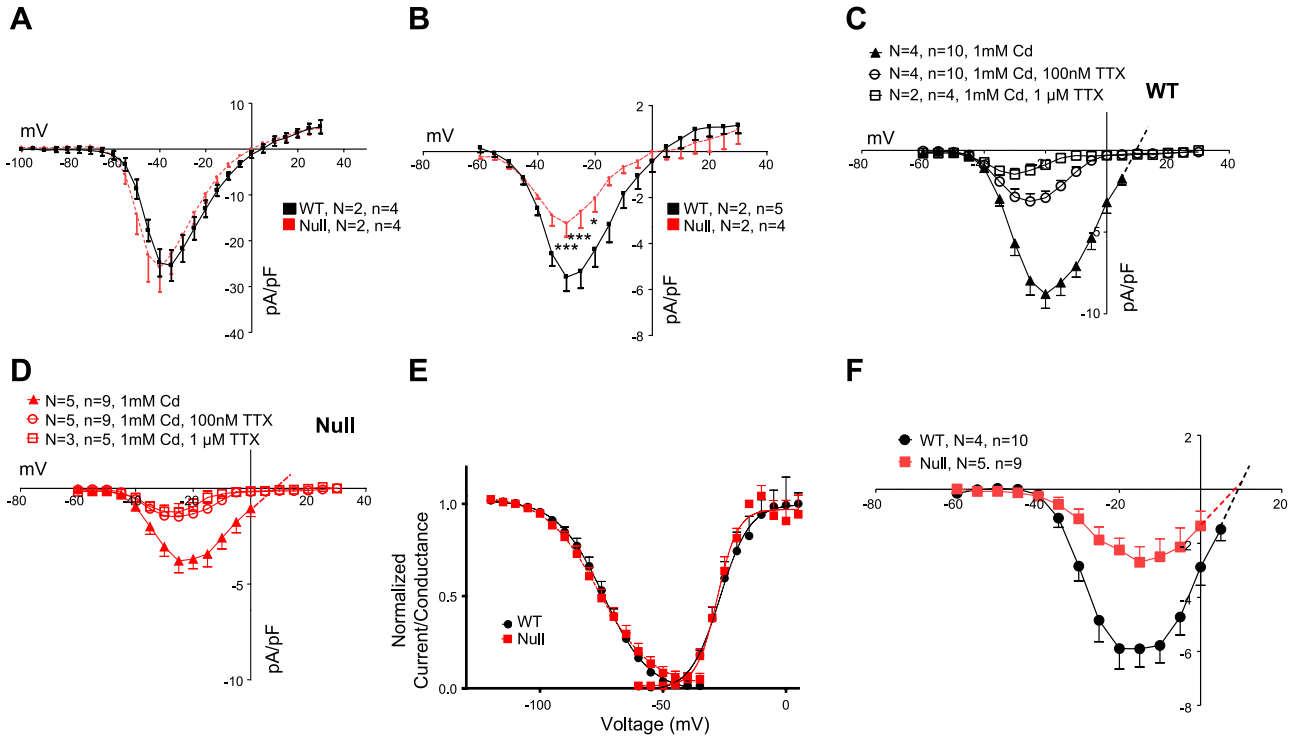

Figure 4. I_{Na} measurement. *A*) Total I_{Na} at HP = −120 mV, $[Na]_o$ = 5mM. *B*) I_{Na} at HP = −70 mV, $[Na]_o$ = 5mM. *C*) I_{Na} at HP = −70 mV with 1 mM Cd^{2+}, and TTX in WT cells, $[Na]_o$ = 50 mM. *D*) I_{Na} at HP = −70 mV with 1 mM Cd^{2+}, and TTX in null cells, $[Na]_o$ = 50 mM. *E*) Steady-state inactivation and activation curves of the sodium current at HP = −70 mV, with 1 mM Cd^{2+}. *F*) TTX (100 nM)-sensitive current obtained from panels *C*, *D*. Data are averages ± SD, ANOVA.

in WT compared with 20 ± 1.2 ms in null ($P<0.05$, ANOVA).

$Na_V1.6$ contributes to conduction velocity and action potential duration in the normal mouse ventricles

In isolated WT and null hearts, we determined the epicardial conduction velocity (CV) and action potential duration (APD) on the anterior surface of the ventricles. Hearts were Langendorff perfused with 4 mM K^+ Tyrode's solution and paced from the apex. Measurements at 2 different cycle lengths (CLs), 140 and 80 ms, demonstrated small but significant differences in both CVs between the two groups. At CL = 140 ms, CV was 61.4 ± 7.2 cm/s in WT hearts (n=16) *vs.* 57.6 ± 4.1 cm/s in null hearts (n=17; $P<0.05$, ANOVA). At CL = 80 ms, CV was 57.5 ± 6.8 ms in WT hearts *vs.* 53.6 ± 5.2 ms in null hearts ($P<0.05$, ANOVA). We also quantified APD_{80}. At CL = 140 ms, APD was 41.2 ± 5.5 ms in WT hearts (n=16) *vs.* 45.6 ± 8.2 ms in null hearts (n=17; $P<0.05$, ANOVA). At CL = 80 ms, APD was 41.3 ± 5.4 ms in WT hearts *vs.* 45.5 ± 5.8 ms in null hearts ($P<0.05$, ANOVA). The plots of these data are not shown. In addition, in subset of 9 WT and 9 null hearts, we investigated the changes in CV and APD as a function of the extracellular potassium concentration ($[K^+]_o$), as described in the following section.

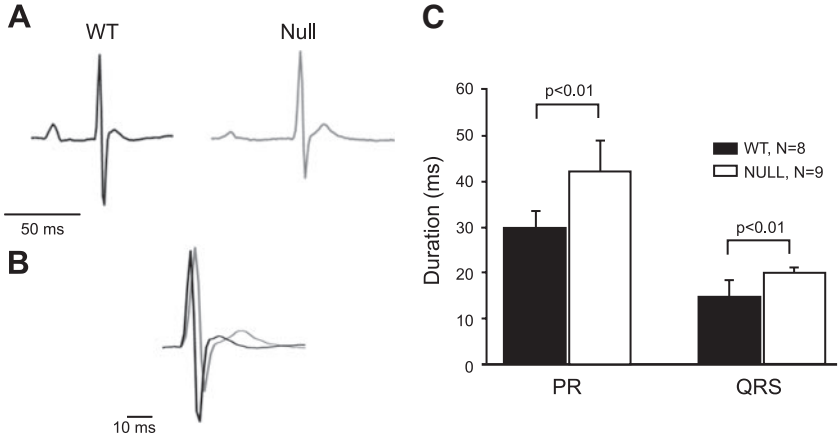

Figure 5. ECG recording. *A*) Representative recordings of a single sinus beat in a WT mouse (left panel) and in a null mouse (right panel). *B*) Superposition of QRS-T complexes from mice in panel *A*. *C*) $Na_V1.6$ mutant mice exhibit prolonged PR and QRS intervals. Data are averages ± SD, ANOVA.

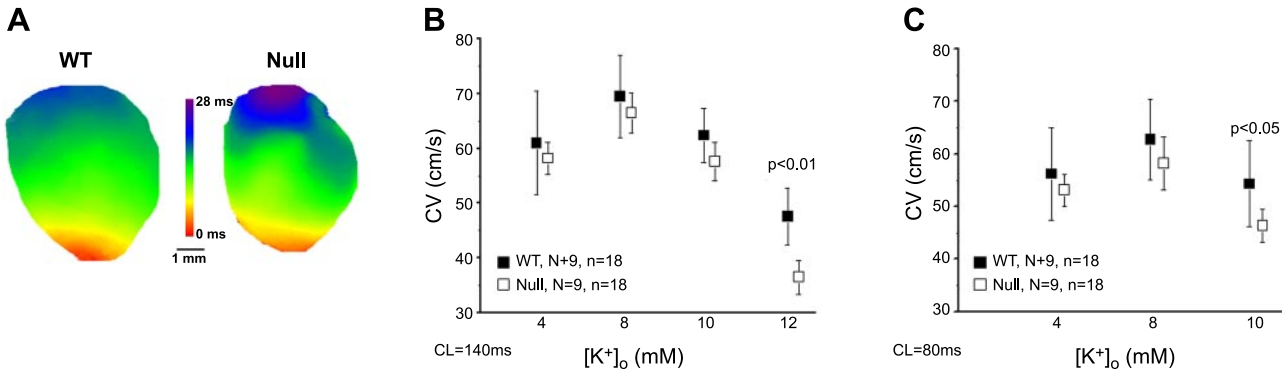

Figure 6. CV in hyperkalemia. *A*) Activation maps of WT and null hearts paced at 140 ms from the apex in 12 mM $[K^+]_o$. *B, C*) Plots of data in 9 WT and 9 null mice at different $[K^+]_o$, with pacing at 140 (*B*) and 80 ms (*C*). Data are averages ± SD, Mixed.

Hyperkalemia exaggerates the slowing of CV in $Na_V1.6$-null mouse hearts

Brain-type sodium channels have more positive activation threshold and greater availability at depolarized ranges of membrane potential than $Na_V1.5$. We therefore surmised that brain-type sodium channels, including $Na_V1.6$, may play a role in helping to maintain impulse conduction in depolarized hearts and that the loss of $Na_V1.6$ should result in a significantly greater reduction of CV than in normally polarized hearts. In 8 WT and 9 null hearts (each heart measured twice), CV was quantified at pacing CL of 140 ms in 4, 8, 10, and 12 mM $[K^+]_o$, and at pacing CL of 80 ms in 4, 8, and 10 mM $[K^+]_o$ (**Fig. 6**). We do not have data during pacing at 80 ms in 12 mM $[K^+]_o$ because 1:1 capture was lost. Figure 6*A* presents activation maps that show an increased time of conduction in null compared to WT hearts during pacing at 140 ms in the presence of 12 mM $[K^+]_o$. Figure 6*B* is a plot of CV (140 ms pacing CL) as a function of $[K^+]_o$. In both WT and null hearts, increasing the $[K^+]_o$ between 4 and 10 mM resulted in a similar biphasic change in CV. However, at 12 mM $[K^+]_o$, CV was 47.6 ± 5.2 cm/s in WT *vs.* 36.5 ± 3.1 cm/s in null hearts. This difference was significant ($P<0.01$, Mixed). Figure 6*C* is a plot of CV at pacing CL of 80 ms. At 4 mM $[K^+]_o$, CV was 56.2 ± 8.8 cm/s in WT *vs.* 53.1 ± 3.1 cm/s in null; and at 8 mM CV increased slightly in both groups of mice. However, at 10 mM $[K^+]_o$, CV was 54.3 ± 8.2 cm/s in WT *vs.* 46.3 ± 3.1 cm/s in null hearts ($P<0.01$, Mixed). These experiments confirm the expected biphasic effects of hyperkalemia on CV (31). Most important, they demonstrate that the absence of $Na_V1.6$ causes a CV defect in the presence of hyperkalemia. It is important to note that due to the smaller number of animals in this experimental subset (8 WT and 9 null), difference in CV was not significant at 4 mM K^+ compared to the significant reduction we observed at 4 mM K^+ in 16 WT and 17 null hearts described in the previous section.

Extracellular potassium and APD

We also quantified the effects of hyperkalemia on APD_{80} (**Fig. 7**). Similarly to CV, APD_{80} was sampled twice in 9 WT and 9 null hearts, at pacing CL of 140 ms in 4, 8, 10, and 12 mM $[K^+]_o$, and at pacing CL of 80 ms in 4, 8, and 10 mM $[K^+]_o$. The representative APD maps in Fig. 7*A* show APD distributions on the anterior wall of the ventricles of representative WT and null hearts paced at CL = 140 ms during 12 mM $[K^+]_o$.

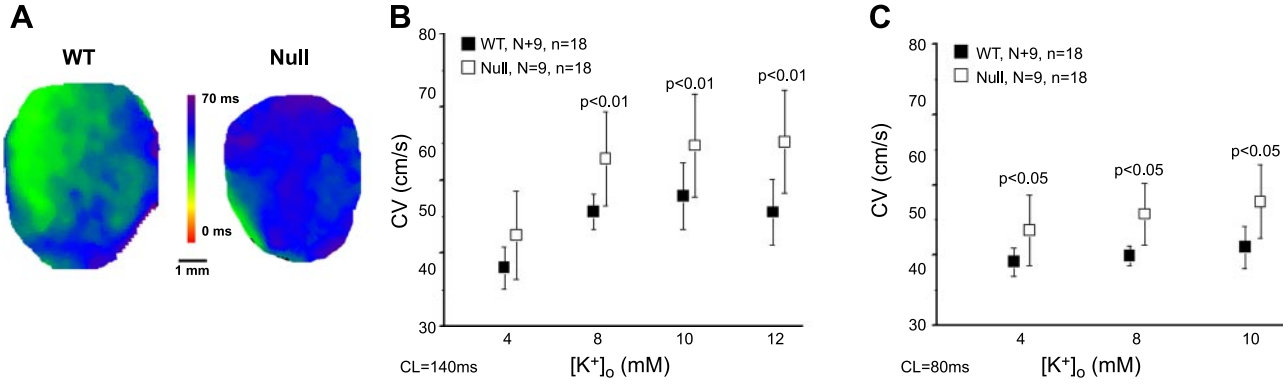

Figure 7. APD_{80} in hyperkalemia. *A*) Anterior surface APD_{80} maps of WT and null hearts paced at 140 ms from the apex in 12 mM $[K^+]_o$. *B, C*) Plot of data in 9 WT and 9 null mice at different $[K^+]_o$, with pacing at 140 (*B*) and 80 ms (*C*). Data are averages ± SD, Mixed.

APD_{80} is prolonged in the null compared to WT hearts. Figure 7*B* is a plot of APD_{80} at 140 ms pacing CL as a function of $[K^+]_o$. APD_{80} increased progressively in both cases, but the increase was significantly steeper for the null hearts. Figure 7*C* shows APD_{80} *vs.* $[K^+]_o$ at pacing CL of 80 ms.

$Na_V1.6$ deletion alters Ca^{2+} transient duration

Brain-type Na^+ channels, including $Na_V1.6$, localize to the t tubules of the ventricular myocyte (ref. 11 and Fig. 3). Some researchers have suggested that brain-type sodium channels contribute to a more effective Ca^{2+}-induced Ca^{2+} release, and consequently to a more efficient contraction, but the idea is controversial (12). We compared the Ca^{2+} transient duration in WT *vs.* null myocytes during pacing at 1Hz. The left panel of **Fig. 8*A*** shows the change in fluorescence along the longitudinal red line on the cartoon of a myocyte. Time-space plots (Fig. 8*A*, center panel) demonstrate that the Ca^{2+} transient duration is longer in the null myocyte. The right panel of Fig. 8*A* shows superimposed Ca^{2+} transient tracings obtained from single camera pixels. The composite plot presented in Fig. 8*B* quantifies the transient durations recorded in 26 cells from 4 WT hearts (357±108 ms) and 28 cells from 4 null hearts (456±84 ms; $P<0.05$, ANOVA). This experiment shows that calcium cycling is altered in $Na_V1.6$ mutant mouse hearts. Whether this is caused by APD prolongation, or because removal of the Nav1.6 from the t tubules causes inefficient and asynchronous calcium cycling and consequently prolongs APD, remains to be determined. Both scenarios are possible. It should also be noted that recently Torres *et al.* (32) showed that neuronal sodium channels contribute to triggering Ca^{2+} release from the sarcoplasmic reticulum in rabbit ventricular myocytes.

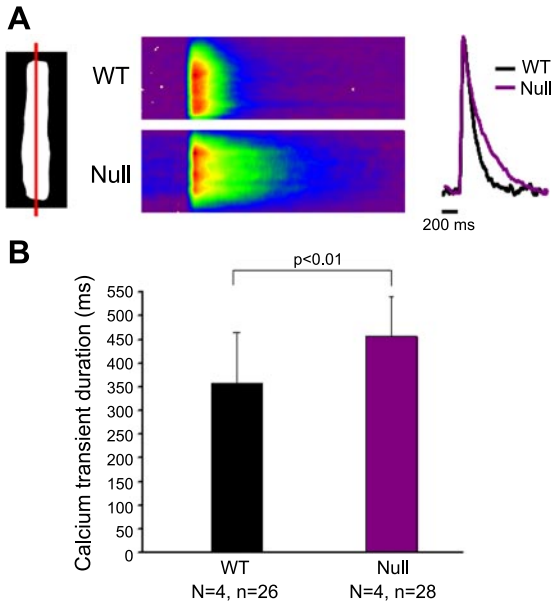

Figure 8. $Na_V1.6$-null mice exhibit a prolonged Ca^{2+} transient. *A*) Left panel: time-space plot line. Center panel: representative time-space plot of Rhod-2 fluorescence in WT (top) and null mouse myocytes (bottom). Right panel: superimposed single-pixel recordings. *B*) Composite plot of Ca^{2+} transients. Data are averages ± SD, ANOVA.

DISCUSSION

The most important results of our study may be summarized as follows: the $Na_V1.6$ transcript encoding the full-length protein is expressed in the mouse ventricles, and the protein is localized mainly in the t tubules of the myocyte; in the NaV1.6-null mice, ventricular myocytes are smaller than in WT, and the TTX-sensitive sodium current is significantly reduced; PR and QRS intervals, as well as ventricular APD, are prolonged in the null mice; at 4 mM $[K^+]_o$, epicardial conduction velocity is slightly reduced, but in hyperkalemia (10 and 12 mM $[K^+]_o$) CV slowing is exaggerated in the null mouse heart; and finally, the calcium transient duration is longer in the null than WT myocytes.

Altogether, the results strongly support the hypothesis that $Na_V1.6$ plays a role in excitation and propagation. Because of its larger availability at more positive membrane potentials compared to the cardiac type $Na_V1.5$ isoform, $Na_V1.6$ may contribute to maintaining the integrity of the action potential propagation when the resting membrane potential is depolarized, such as in hyperkalemia. In addition, because of their localization at the t tubules, $Na_V1.6$ channels likely participate in EC coupling by accelerating the depolarization of the sarcolemmal membrane, and thus synchronizing the calcium-induced calcium-release events.

$Na_V1.6$ channels are encoded by the *SCN8A* gene, which was originally identified by positional cloning of a mouse mutant (33). When expressed in nonexcitable cells in culture, the voltage-dependent activation and fast inactivation properties of $Na_V1.6$ are similar to $Na_V1.2$, but its voltage dependence of slow inactivation is more positive than other brain-type Na^+ channels (22). Estimates using various pharmacologic strategies indicate that between 5 and 8% of the total cardiac I_{Na} originates from brain-type TTX-sensitive sodium channels in ventricular myocytes in mice (11, 20, 21), 11% in rats, and 10% in dogs, (20), and 20% in cardiac Purkinje cells in dogs (20). The Catterall laboratory (11) has recorded neuronal Na^+ current in cardiac myocytes using a scorpion toxin activator of these channels. However, to our knowledge, our study is the first to focus on the specific role played by $Na_V1.6$ in cardiac electrical function using genetically altered mice. Since brain-type sodium channels, particularly $Na_V1.6$, display a greater availability than $Na_V1.5$ at positive potentials (3) they are adequately suited to maintain excitability in the more depolarized cardiac muscle. This is clearly the case in isolated $Na_V1.6$ mutant mice exposed to high extracellular potassium concentrations (Fig. 6). In addition, it is reasonable to surmise that the unusually large late component of the sodium current of $Na_V1.6$ (22) contributes to APD in

the heart. However, APD is prolonged in the null mice. Such a counterintuitive prolongation may be brought about by potassium-channel remodeling, such as the transient outward current I_{to}, $I_{KSlow,}$ the sustained current I_{Ksus}, or the inward rectifier current I_{K1}. It could also be a response to the prolonged Ca^{2+} transient and the activation of the Na-Ca exchange current.

Brain-type sodium channels and EC coupling

Maier *et al.* (11) demonstrated that nanomolar concentrations of TTX interfered with left ventricular contractile function. The researchers proposed that brain-type sodium channels play a role in coupling depolarization of the cell surface membrane to contraction. Torres *et al.* (32) also suggested that neuronal sodium channels are important for EC coupling in the rabbit ventricular myocyte. Other researchers disagree (12). Our experiments in $Na_V1.6$ mutant mice clearly show a prolongation of the Ca^{2+} transient duration (Fig. 8), indicating some kind of EC coupling disruption. Additional work is required to investigate these issues. The prolongation of the calcium transient in the $Na_V1.6$-null mice opens new avenues for research into its underlying mechanisms. It may be caused by delays in the triggering of Ca^{2+} release (29), late-opening LCCs, slowly propagating calcium induced calcium release waves, or slowed reuptake of cytosolic Ca^{2+} due to changes in the SERCA pump, phospholamban, or the sodium calcium exchanger.

Pathophysiological implications

TTX-sensitive brain-type Na^+ channels appear to contribute to automaticity of sinoatrial nodal cells of the mouse heart and may have a role in sinoatrial dysfunction (13). Recently it was shown that $Na_V1.1$ and $Na_V1.6$ are the primary Na^+-channel subunits in the rat sinus node and that heart failure results in their downregulation (14). Missense mutations of neuronal Na^+-channel genes have been linked to epilepsy, chronic pain, and migraine, and >700 mutants of Nav1.1 have been identified in patients with epilepsy (4, 34, 35). In many cases, the defect not only increases the late component of the current in neurons but may also have life-threatening consequences in the heart because of prolongation of the QT interval (3), although no direct link between LQT and neuronal sodium-channel mutations has been made. It is interesting that QT prolongation is thought to be a major mechanism leading to sudden unexpected death in epilepsy (36). In addition, ictal atrioventricular block is a common finding in patients with epilepsy, and QT dispersion, a risk indicator of cardiac arrhythmias, is significantly increased on ECG of children with epilepsy (3). A heterozygous null mutation of human $Na_V1.6$ was identified in a family with ataxia and cognitive impairment (5); however, it is not known whether the patients present a cardiac phenotype. Our results provide the first direct demonstration that a brain-type sodium-channel mutation that results in severe ataxia in the mouse also has cardiac consequences, including alterations in cardiac impulse conduction and EC-coupling synchrony. Whether those cardiac consequences are significant in patients with equivalent brain-type mutations remains to be determined.

Limitations

Many differences exist between ion channels that underlie the action potential waveforms in rodents and humans, which calls for extreme caution before attempting to extrapolate our results. Our analysis has been restricted to very young mice because of the lethality of the $Na_V1.6$-null mutation at 3 wk of age (18). In addition, the global $Na_V1.6$-null mice may exhibit secondary effects on the heart, such as lateralization of connexin43, possible compensatory changes in other neuronal sodium channels, or adaptive remodeling due to the decreased body size of the null mice. For these reasons, development of a heart-specific $Na_V1.6$-KO mouse model should be valuable for confirming the cell-autonomous role of $Na_V1.6$ in cardiomyocytes and characterization of $Na_V1.6$ deficiency in the adult heart.

CONCLUSIONS

The demonstration that brain-type Na^+ channels are expressed in various proportions in the heart, and that they contribute to function in most cardiac tissues, including sinoatrial node, (13) ventricles (11, 12, 21), and cardiac conduction system, (20) has opened new and exciting pathways for research into the molecular basis of cardiac excitability and arrhythmogenesis in both cardiac and brain diseases. Characterization of new models of brain-type ion-channel diseases in mice offers unique opportunities to better understand the molecular mechanisms of cardiac disease pathogenesis associated with imbalances of specific ion-channel isoforms. Previous functional studies of the brain-type channels in heart have relied on the pharmacological distinction between cardiac and brain channels, (3), based on the greater sensitivity of the brain channels to TTX compared to the cardiac $Na_V1.5$ channels. However, TTX sensitivity does not distinguish among the brain channels $Na_V1.1$, $Na_V1.3$, and $Na_V1.6$, all of which seem to be expressed in the heart. Our demonstration of a cardiac phenotype in $Na_V1.6$-null mice provides the first direct evidence for the importance of $Na_V1.6$ in EC coupling and in the maintenance of ventricular conduction velocity and possibly under conditions in which the resting membrane potential is depolarized and cardiac excitability is jeopardized. FJ

Supported by U.S. National Heart, Blood, and Lung Institute grants P01-HL039707 and P01-HL087226 (J.J.) and K99-HL105574 (S.F.N.), the Leducq Foundation (J.J.), and National Institute of Neurological Disorders and Stroke grant R01-NS34509 (M.M.). The authors thank Dr. Nidhi Talwar (Center for Statistical Consultation and Research, University of Michigan).

REFERENCES

1. Priori, S. G., and Napolitano, C. (2004) Genetics of cardiac arrhythmias and sudden cardiac death. *Ann. N. Y. Acad. Sci.* **1015,** 96–110
2. Sauer, A. J., Moss, A. J., McNitt, S., Peterson, D. R., Zareba, W., Robinson, J. L., Qi, M., Goldenberg, I., Hobbs, J. B., Ackerman, M. J., Benhorin, J., Hall, W. J., Kaufman, E. S., Locati, E. H., Napolitano, C., Priori, S. G., Schwartz, P. J., Towbin, J. A., Vincent, G. M., and Zhang, L. (2007) Long QT syndrome in adults. *J. Am. Coll. Cardiol.* **49,** 329–337
3. Haufe, V., Chamberland, C., and Dumaine, R. (2007) The promiscuous nature of the cardiac sodium current. *J. Mol. Cell. Cardiol.* **42,** 469–477
4. Catterall, W. A., Dib-Hajj, S., Meisler, M. H., and Pietrobon, D. (2008) Inherited neuronal ion channelopathies: new windows on complex neurological diseases. *J. Neurosci.* **28,** 11768–11777
5. Trudeau, M. M., Dalton, J. C., Day, J. W., Ranum, L. P., and Meisler, M. H. (2006) Heterozygosity for a protein truncation mutation of sodium channel SCN8A in a patient with cerebellar atrophy, ataxia, and mental retardation. *J. Med. Genet.* **43,** 527–530
6. Yu, F. H., and Catterall, W. A. (2004) The VGL-chanome: a protein superfamily specialized for electrical signaling and ionic homeostasis. *Sci. STKE* **2004,** re15
7. Goldin, A. L., Barchi, R. L., Caldwell, J. H., Hofmann, F., Howe, J. R., Hunter, J. C., Kallen, R. G., Mandel, G., Meisler, M. H., Netter, Y. B., Noda, M., Tamkun, M. M., Waxman, S. G., Wood, J. N., and Catterall, W. A. (2000) Nomenclature of voltage-gated sodium channels. *Neuron* **28,** 365–368
8. Catterall, W. A. (1984) The molecular basis of neuronal excitability. *Science* **223,** 653–661
9. Maier, S. K., Westenbroek, R. E., McCormick, K. A., Curtis, R., Scheuer, T., and Catterall, W. A. (2004) Distinct subcellular localization of different sodium channel alpha and beta subunits in single ventricular myocytes from mouse heart. *Circulation* **109,** 1421–1427
10. Lopez-Santiago, L. F., Meadows, L. S., Ernst, S. J., Chen, C., Malhotra, J. D., McEwen, D. P., Speelman, A., Noebels, J. L., Maier, S. K., Lopatin, A. N., and Isom, L. L. (2007) Sodium channel Scn1b null mice exhibit prolonged QT and RR intervals. *J. Mol. Cell. Cardiol.* **43,** 636–647
11. Maier, S. K., Westenbroek, R. E., Schenkman, K. A., Feigl, E. O., Scheuer, T., and Catterall, W. A. (2002) An unexpected role for brain-type sodium channels in coupling of cell surface depolarization to contraction in the heart. *Proc. Natl. Acad. Sci. U. S. A.* **99,** 4073–4078
12. Brette, F., and Orchard, C. H. (2006) No apparent requirement for neuronal sodium channels in excitation-contraction coupling in rat ventricular myocytes. *Circ. Res.* **98,** 667–674
13. Maier, S. K., Westenbroek, R. E., Yamanushi, T. T., Dobrzynski, H., Boyett, M. R., Catterall, W. A., and Scheuer, T. (2003) An unexpected requirement for brain-type sodium channels for control of heart rate in the mouse sinoatrial node. *Proc. Natl. Acad. Sci. U. S. A.* **100,** 3507–3512
14. Du, Y., Huang, X., Wang, T., Han, K., Zhang, J., Xi, Y., Wu, G., and Ma, A. (2007) Downregulation of neuronal sodium channel subunits Nav1.1 and Nav1.6 in the sinoatrial node from volume-overloaded heart failure rat. *Pflügers Arch.* **454,** 451–459
15. Meisler, M. H., Plummer, N. W., Burgess, D. L., Buchner, D. A., and Sprunger, L. K. (2004) Allelic mutations of the sodium channel SCN8A reveal multiple cellular and physiological functions. *Genetica* **122,** 37–45
16. Cote, P. D., De Repentigny, Y., Coupland, S. G., Schwab, Y., Roux, M. J., Levinson, S. R., and Kothary, R. (2005) Physiological maturation of photoreceptors depends on the voltage-gated sodium channel NaV1.6 (Scn8a). *J. Neurosci.* **25,** 5046–5050
17. De Repentigny, Y., Cote, P. D., Pool, M., Bernier, G., Girard, S., Vidal, S. M., and Kothary, R. (2001) Pathological and genetic analysis of the degenerating muscle (dmu) mouse: a new allele of Scn8a. *Hum. Mol. Genet.* **10,** 1819–1827
18. Sharkey, L. M., Cheng, X., Drews, V., Buchner, D. A., Jones, J. M., Justice, M. J., Waxman, S. G., Dib-Hajj, S. D., and Meisler, M. H. (2009) The ataxia3 mutation in the N-terminal cytoplasmic domain of sodium channel Na(v)1.6 disrupts intracellular trafficking. *J. Neurosci.* **29,** 2733–2741
19. Cerrone, M., Noujaim, S. F., Tolkacheva, E. G., Talkachou, A., O'Connell, R., Berenfeld, O., Anumonwo, J., Pandit, S. V., Vikstrom, K., Napolitano, C., Priori, S. G., and Jalife, J. (2007) Arrhythmogenic mechanisms in a mouse model of catecholaminergic polymorphic ventricular tachycardia. *Circ. Res.* **101,** 1039–1048
20. Haufe, V., Cordeiro, J. M., Zimmer, T., Wu, Y. S., Schiccitano, S., Benndorf, K., and Dumaine, R. (2005) Contribution of neuronal sodium channels to the cardiac fast sodium current INa is greater in dog heart Purkinje fibers than in ventricles. *Cardiovasc. Res.* **65,** 117–127
21. Brette, F., and Orchard, C. H. (2006) Density and sub-cellular distribution of cardiac and neuronal sodium channel isoforms in rat ventricular myocytes. *Biochem. Biophys. Res. Commun.* **348,** 1163–1166
22. Chen, Y., Yu, F. H., Sharp, E. M., Beacham, D., Scheuer, T., and Catterall, W. A. (2008) Functional properties and differential neuromodulation of Na(v)1.6 channels. *Mol. Cell. Neurosci.* **38,** 607–615
23. Heinemann, S. H., Terlau, H., and Imoto, K. (1992) Molecular basis for pharmacological differences between brain and cardiac sodium channels. *Pflügers Arch.* **422,** 90–92
24. Vaidya, D., Morley, G. E., Samie, F. H., and Jalife, J. (1999) Reentry and fibrillation in the mouse heart. A challenge to the critical mass hypothesis. *Circ. Res.* **85,** 174–181
25. Noujaim, S. F., Pandit, S. V., Berenfeld, O., Vikstrom, K., Cerrone, M., Mironov, S., Zugermayr, M., Lopatin, A. N., and Jalife, J. (2007) Up-regulation of the inward rectifier K+ current (I K1) in the mouse heart accelerates and stabilizes rotors. *J. Physiol.* **578,** 315–326
26. Morley, G. E., Vaidya, D., and Jalife, J. (2000) Characterization of conduction in the ventricles of normal and heterozygous Cx43 knockout mice using optical mapping. *J. Cardiovasc. Electrophysiol.* **11,** 375–377
27. Morley, G. E., Vaidya, D., Samie, F. H., Lo, C., Delmar, M., and Jalife, J. (1999) Characterization of conduction in the ventricles of normal and heterozygous Cx43 knockout mice using optical mapping. *J. Cardiovasc. Electrophysiol.* **10,** 1361–1375
28. Vaitkevicius, R., Saburkina, I., Rysevaite, K., Vaitkeviciene, I., Pauziene, N., Zaliunas, R., Schauerte, P., Jalife, J., and Pauza, D. H. (2009) Nerve supply of the human pulmonary veins: an anatomical study. *Heart Rhythm* **6,** 221–228
29. Song, L. S., Sobie, E. A., McCulle, S., Lederer, W. J., Balke, C. W., and Cheng, H. (2006) Orphaned ryanodine receptors in the failing heart. *Proc. Natl. Acad. Sci. U. S. A.* **103,** 4305–4310
30. Plummer, N. W., McBurney, M. W., and Meisler, M. H. (1997) Alternative splicing of the sodium channel SCN8A predicts a truncated two-domain protein in fetal brain and non-neuronal cells. *J. Biol. Chem.* **272,** 24008–24015
31. Kleber, A. G., and Rudy, Y. (2004) Basic mechanisms of cardiac impulse propagation and associated arrhythmias. *Physiol. Rev.* **84,** 431–488
32. Torres, N. S., Larbig, R., Rock, A., Goldhaber, J. I., and Bridge, J. H. (2010) Na+ currents are required for efficient excitation-contraction coupling in rabbit ventricular myocytes: a possible contribution of neuronal Na+ channels. *J. Physiol.* **588,** 4249–4260
33. Burgess, D. L., Kohrman, D. C., Galt, J., Plummer, N. W., Jones, J. M., Spear, B., and Meisler, M. H. (1995) Mutation of a new sodium channel gene, Scn8a, in the mouse mutant 'motor endplate disease.' *Nat. Genet.* **10,** 461–465
34. Meisler, M. H., O'Brien, J. E., and Sharkey, L. M. (2010) The sodium channel gene family: epilepsy mutations, gene interactions and modifier effects. *J. Physiol.* **588,** 1841–1848
35. Meisler, M. H., and Kearney, J. A. (2005) Sodium channel mutations in epilepsy and other neurological disorders. *J. Clin. Invest.* **115,** 2010–2017
36. Christidis, D., Kalogerakis, D., Chan, T. Y., Mauri, D., Alexiou, G., and Terzoudi, A. (2006) Is primidone the drug of choice for epileptic patients with QT-prolongation? A comprehensive analysis of literature. *Seizure* **15,** 64–66
37. Nerbonne, J. M. (2000) Molecular basis of functional voltage-gated K+ channel diversity in the mammalian myocardium. *J. Physiol.* **525**(Pt. 2), 285–298

Received for publication January 13, 2011
Accepted for publication September 1, 2011.